Published in final edited form as:
Comput Struct. 2007 ; 85(11-14): 1012–1019. doi:10.1016/j.compstruc.2006.11.018.

Flow over a membrane-covered, fluid-filled cavity

Scott L. Thomson[*], **Luc Mongeau**[**], and **Steven H. Frankel**[**]

Scott L. Thomson: thomson@byu.edu

[*]Department of Mechanical Engineering, Brigham Young University, Provo, UT, 84602, Ph. 1-801-422-4980. Fax: 1-801-422-0516

[**]School of Mechanical Engineering, Purdue University, 585 Purdue Mall, West Lafayette, IN 47907-2040

Abstract

The flow-induced response of a membrane covering a fluid-filled cavity located in a section of a rigid-walled channel was explored using finite element analysis. The membrane was initially aligned with the channel wall and separated the channel fluid from the cavity fluid. As fluid flowed over the membrane-covered cavity, a streamwise-dependent transmural pressure gradient caused membrane deformation. This model has application to synthetic models of the vocal fold cover layer used in voice production research. In this paper, the model is introduced and responses of the channel flow, the membrane, and the cavity flow are summarized for a range of flow and membrane parameters. It is shown that for high values of cavity fluid viscosity, the intracavity pressure and the beam deflection both reached steady values. For combinations of low cavity viscosity and sufficiently large upstream pressures, large-amplitude membrane vibrations resulted. Asymmetric conditions were introduced by creating cavities on opposing sides of the channel and assigning different stiffness values to the two membranes. The asymmetry resulted in reduction in or cessation of vibration amplitude, depending on the degree of asymmetry, and in significant skewing of the downstream flow field.

1. Introduction

Compliant-walled channels have been the subject of numerous experiments and computational simulations because of their possible applications to the study of diverse biological systems. In these studies, a deformable structure, such as a stretched membrane, replaces the rigid wall of a channel or a tube over a finite region along the streamwise direction; this is illustrated in Fig. 1. Typically, a constant pressure is applied to the membrane exterior and the structure deforms in response to the transmural pressure gradient. Depending on membrane and flow parameters, large-scale deformation may result, often accompanied by self-sustained oscillations. Detailed studies of such phenomena can be found in the literature [1–9]. In the present study, a modification of this model was used to investigate vocal fold vibration. Before introducing the model, an introduction to the vocal fold system is here provided.

Correspondence to: Scott L. Thomson, thomson@byu.edu.

The vocal folds are masses of multiple, connected tissue layers located within the larynx; Figure 2 illustrates a cross section of the vocal folds. The tissue layers are of varying composition and structural properties. The vocal fold outermost layer (that lines the tracheal lumen) is a thin epithelial layer. Just deep to the epithelium is the lamina propria, which in turn is comprised of three layers: superficial, intermediate, and deep. Finally, a layer of muscle comprises the bulk of the vocal fold. Following the body-cover model of the vocal fold structure [10], the "cover" denotes the combined epithelium and superficial lamina propria, the ligament consists of the intermediate and deep layers of the lamina propria, and the body denotes the muscle layer. These are illustrated in Fig. 2.

The stiffness of the different layers varies. The Young's moduli are generally believed to be on the order of $10^4 - 10^7$ Pa for the epithelium, $10^2 - 10^3$ Pa for the superficial lamina propria, 10^4 Pa for the ligament, and $10^4 - 10^5$ Pa for the muscle. The epithelium constitutes only a relatively minor portion, geometrically speaking, of the cover, with a thickness on the order of 50 μm [10], compared to about 1 mm for the cover. The epithelium is structurally necessary, however, to support the highly compliant superficial lamina propria.

During rest, the vocal folds are open, allowing for air exchange between the lungs and the external environment. During speech, the vocal folds are adducted and lung airflow increases; this combination results in a flow-induced vibration of the vocal folds. Although some motion of the ligament and body layers occurs, most of the vibration typically occurs in the cover layer. The vibration takes the general form of a surface wave traveling vertically along the vocal fold medial surface; it is commonly referred to as a "mucosal wave." Vocal fold vibration occurs at frequencies ranging from about 100 to 1000 Hz at amplitudes on the order of 1 mm. Typically, the vocal folds collide and remain in contact for about 50% of the oscillation cycle. The vocal fold system is, therefore, from a scientific perspective, rich with applications in fluid mechanics, structural dynamics, and acoustics. From a clinical standpoint, rigorous study of vocal fold vibration has the potential to be of great benefit to speech clinicians and surgeons.

Numerous numerical and physical models have been used to study the vocal folds. Experimental models have included continuum models [11] and models of the epithelium and superficial lamina propria [12–14]. Computational models have ranged from reduced-order models that represent the vocal folds as systems of spring-coupled masses driven by one-dimensional flow models [15], to more complex two- and three-dimensional finite element models [11, 16–20].

The vocal folds of the finite element models have often been represented using the cover-ligament-body structure. However, in order to develop further understanding of the vibration of the vocal fold cover region, a more focused two-layer model of the vocal fold cover is necessary. This is in order to separately model the epithelium and superficial lamina propria. Such a model is the focus of the present study.

The "canonical" model of a membrane in a channel wall was modified to simulate the vocal fold cover. Whereas in the aforementioned membrane-channel cases a constant pressure was applied to the membrane exterior (on the "non-flow" side), in the present case, a fluid cavity of finite volume was defined along the membrane exterior. The fluid cavity region represented the superficial lamina propria and the beam represented the epithelium; together, these represented the vocal fold cover. This concept has been utilized before in experimental models of the vocal fold cover [12–14]. In these models, a thin silicone membrane (representing the epithelium) was attached to a rigid base (representing the body), and a fluid (representing the superficial lamina propria) was injected into the space in between the membrane and the base. The physical model was used in a hemilarynx configuration (only

one vibrating vocal fold), in part because creating two precisely symmetric models using this technique was very difficult. This model was previously used to investigate phonation onset pressure for varying values of fluid, solid, and geometrical parameters [12–14].

In the present study, the numerical model was used to investigate the influence of glottal width and the influence of asymmetry in membrane stiffness on vibrations. The numerical model was well-suited for this purpose since the degree of asymmetry could be precisely controlled.

2. Numerical Methods

2.1. Model Description

The two-dimensional domain, shown in Fig. 3, was used to simulate the larynx, including the vocal fold region. Note the coordinate system definition (defined as such for consistency with the vocal fold modeling literature). A rigid-walled constriction represented the vocal fold body, and beam-covered cavities representing the two vocal fold covers were placed at the narrowest point of the constriction.

Table 1 summarizes the flow and structural parameters used in the model. The cavity dimensions were AC = BD = 1.25 mm and AB = CD = 6.7 mm; the cavity dimensions were symmetric about $z = 0$. The glottal gap d_g ranged from 0.25 mm to 1 mm. The channel height, H, was 5.4 cm; this is approximately twice that of the human larynx, but corresponded to the height of the distance of earlier synthetic hemilarynx cover model studies [12–14]. The dimension of d_g was taken as the resting (no-flow state) distance between the beams. The inlet was located 6.6 cm upstream of A; the outlet was located 30 cm downstream of B. It is noted that for computational efficiency, only one half of the domain was modeled for the symmetric cases.

2.1.1. Solid Domain—The structural domain consisted of two separate beams that covered the cavities, denoted as the “top” and “bottom” beams and cavities (identified in Fig. 3). The density and Poisson’s ratio of each beam was $\rho_s = 1500$ kg/m^3 and $\nu = 0.45$, respectively. The beam endpoints were rigidly fixed to the channel walls (zero displacement and zero rotation endpoint boundary conditions). The Young’s modulus of the bottom beam was fixed at $E_B = 5\times10^5$ Pa. It is noted that Kakita et al. [20] found Young’s modulus values of the canine epithelium to be on the order of $10^6 – 10^7$ Pa. However, it is possible that these measurements yielded artificially high values because of limitations in the experimental apparatus, and recent data suggests that the Young’s modulus of the human epithelium may range from about 2×10^4 Pa at low strain to 10^5 Pa at high (25%) strain [21]. Further investigation remains necessary to precisely determine the range of Young’s modulus values found in human vocal fold epithelium. The modulus values chosen in this simulation, therefore, represent an intermediate value of the available data.

The top beam Young’s modulus was varied from $E_T = 5\times10^5$ Pa to 5×10^6 Pa, such that the ratio of the Young’s modulus of the top beam to that of the bottom beam, $E^* = E_T/E_B$, ranged from $E^* = 1$ to $E^* = 10$. The beam thickness was 0.05 mm to match that of the human vocal fold epithelium. No material damping was applied in the structural domain.

The rectangular cavity in the numerical model below the beam did not extend along the full inferior-superior (z – direction) length of the vocal fold medial surface, whereas in the earlier physical models [12–14], the entire medial surface was compliant. This was done primarily to avoid possible complications arising from buckling of the beam due to compressive forces.

2.1.2. Channel Fluid Domain—The channel fluid, representing air flowing from the lungs through the vocal tract, was modeled as an incompressible gas with density $\rho_p = 1.2$ kg/m^3 and viscosity $\mu_p = 1.8\times10^{-5}$ kg/(m·s). The pressure at the downstream exit was fixed at $p_d = 0$ Pa. Simulations were performed with the inlet pressure ranging from $p_i = 10$ Pa to $p_i = 500$ Pa. These resulted in steady flow Reynolds numbers in the range of approximately 20 to 80 (based on the inlet channel height and on the inlet channel velocities corresponding to the applied pressures). The no-slip boundary condition was applied along all walls and along the beams.

2.1.3. Cavity Fluid Domain—The fluid within the cavity had a density of $\rho_c = 1000$ kg/m^3 and variable viscosity; both cavities were defined using the same fluid properties. Separate simulations were performed to determine the steady and unsteady beam deformation behavior. In the steady cases, a true "steady-state" simulation was not possible since the pressure within the deformed cavity was unknown. Therefore, to predict the steady beam deformation, the cavity fluid viscosity was set to a relatively large value [$\mu_c = 10^{-1}$ kg/(m·s)] to suppress oscillations. A time-marching simulation was then performed with the cavity initially undeformed and the fluid in all domains initially at rest. These simulations are referred to as "steady, overdamped" since cavity fluid damping caused the beam to quickly reach a stationary, deformed position.

When the beam oscillations were of interest, the fluid viscosity was lowered to that of water [$\mu_c = 10^{-3}$ kg/(m·s)]. In these transient simulations, the steady solution was used to provide the initial conditions for the unsteady solution, and a perturbation was applied to trigger oscillations by briefly increasing the inlet pressure at the beginning of the unsteady simulations. These simulations are referred to as "transient" since the oscillations of the beam were studied.

2.1.4. Fluid-Beam Interface—Since the beam was in contact with both fluid domains, one fluid-structure interface was defined along the beam-channel fluid interface and another was defined along the beam-cavity fluid interface. The no-slip boundary condition dictated that the fluid velocity at the fluid-structure interfaces in both fluid domains was equal to that of the beam velocity. The channel and cavity fluid domains were meshed separately to prevent sharing of nodes along the beam-fluid interfaces.

2.2. Numerical Methods

The computational simulations were performed by implementing the finite element method [22–25] using the commercial code ADINA (ADINA R&D, Boston, Massachusetts). ADINA is a finite element code dedicated to the solution of fully-coupled fluid-structure interaction problems and has been used in previous collapsible channel studies [7,8]. Grid refinement and time step studies were performed to verify grid and time-step independence. In summary, the fluid domain consisted of just over 50,000 3-node triangular elements and 26,000 nodes. Each beam was modeled using 100 3-node isoparametric plane strain beam elements and calculations were carried out under the assumptions of large deformation and small strain. A time step size of 10^{-4} s was used with a second-order trapezoidal rule time marching scheme.

3. Results

3.1. Influence of Initial Gap Width

3.1.1. Steady, Overdamped Response—Flow over the cavity resulted in the familiar beam profile seen in previous collapsible channel studies; this is shown in Fig. 4 for the case of $p_i = 30$ Pa and symmetric conditions. The upstream portion of the beam was expanded,

similar to that of the pressure-loaded beam. However, because the fluid inside each cavity was incompressible, the total cavity volume (or area per unit depth) was constant. This created the condition that any outward movement of some region of the beam had to be accompanied by a corresponding inward movement of some other region of the beam. Thus unlike the constant pressure-loaded beam cases, the fluid-loaded beam always possessed an inflection point between convex and concave regions. Further, in the present cases, the pressure within the cavity reached a uniform steady value. This is also shown in Fig. 4, where the steady cavity pressure was approximately 18 Pa.

The steady displacement of the beam, normalized by the initial orifice width, d_g, is shown in Fig. 5 for different values of d_g. As d_g was reduced, the beam deformation relative to d_g increased. However, the absolute deformation showed a slightly different trend, as can be seen in Fig. 6, in which the maximum and minimum beam displacements are shown for different values of d_g. As d_g decreased from 1 mm, the displacement initially gradually increased, but then slightly decreased for $d_g < 0.5$ mm as viscous effects began to be significant.

3.1.2. Time-Varying Response—The stability of the beam with a subglottal pressure of $p_s = 30$ Pa was investigated for three different values of d_g. The results are shown in Fig. 7, in which the location of a node on the beam was followed; the coordinates of the point at $t = 0$ coincide with the points for $E^* = 1$ listed in Table 2. The oscillations were self-sustained for $d_g = 0.5$ mm, but decayed for all other cases. The steady-state peak-to-peak oscillation amplitude for $d_g = 0.5$ mm was 0.16 mm, or 32% of the gap height, and the frequency of oscillation was approximately 72 Hz.

Note is here made of the experimental observations of Titze et al. [12] and Chan et al. [13], in which the influence of the prephonatory glottal width, d_g, on phonation onset pressure was investigated. It was found that for sufficiently large values of d_g, the onset pressure increased as d_g decreased; this was in agreement with theoretical predictions [26]. For very small values of d_g (i.e., on the order of 0.2 mm as shown by Lucero [27]), intraglottal viscous effects became significant, resulting in increases in onset pressure with further decreases in d_g. One implication of these experimental results is that for a fixed upstream pressure (within a certain range), there also exists a range of initial glottal widths for which oscillations will occur. Glottal widths outside of this range will not produce oscillations, owing to either insufficient aerodynamic energy to maintain oscillations (for large widths) or to too much viscous energy dissipation (for small widths). The present model's behavior is consistent with this observation. The lack of model vibration at $d_g = 1$ mm is attributed to insufficient aerodynamic energy, and the lack of vibration at $d_g = 0.25$ mm is attributed to the viscous energy dissipation being sufficiently great so as to reduce the energy available for sustained vibrations.

For the unsteady cases, the pressure within the cavity was no longer uniform. This is evident in Fig. 8, where the beam and fluid domains are shown at several different times during one period of oscillation. These figures correspond to one cycle after steady-state vibrations had been achieved. The motion of the fluid within the cavity resulted in significantly non-uniform cavity pressure fields.

3.2. Influence of Subglottal Pressure

The influence of the subglottal pressure on the steady and unsteady deformation was investigated. The initial orifice width for these cases was $d_g = 0.5$ mm.

3.2.1. Steady, Overdamped Response—The steady beam displacement was predicted for values of subglottal pressure ranging from p_s = 10 to p_s = 500 Pa, and the results are shown in Fig. 9. For p_s = 10 Pa, the beam deflection was nearly anti-symmetric about its midpoint. As the pressure was increased, the constriction narrowed and moved downstream, while the expansion grew slightly and also moved downstream, although the displacement of the constricted region was more pronounced than that of the expanded region. At p_s = 500 Pa, beam deformation had resulted in orifice occlusion of more than 90% of the initial orifice width.

3.2.2. Time-Varying Response—Figure 10 shows the beam position for two cases, p_s = 10 Pa and p_s = 30 Pa. At the lower pressure, the oscillations were negligible and quickly decayed. Steady-state oscillations were reached for p_s = 30 Pa. It was found that oscillations were unstable for p_s > 100 Pa; the relatively small operating pressure range was attributed to the absence of damping in the structural domain. The subglottal pressure value of p_s = 30 Pa is approximately one-tenth of the onset pressure required for human speech. This relatively low onset pressure is also attributed to the absence of material damping in the beam model, as well as to the difference in damping in the fluid-filled cavity and damping within superficial lamina propria tissue. In the human vocal folds, significant material damping is present in the vocal fold tissue, whereas in the numerical model, damping was limited to viscous losses in the fluid domains. It is expected that increased damping in the fluid and beam regions would result in increased onset pressure and reduced vibration frequency, although further studies would be required to confirm this hypothesis. Further studies into the relative contributions of damping in the beam and fluid regions to the overall energy dissipation would also be beneficial.

3.3. Influence of Asymmetry in Beam Stiffness

Model asymmetry was investigated by varying the Young's modulus of one beam while holding that of the other beam constant. Both steady and unsteady cases were investigated. In the human vocal folds, mild asymmetry in tissue properties may be present under normal (healthy) conditions, and more extreme asymmetry may result from scarring, benign lesions, and surgically-induced modifications to correct for unilateral vocal fold paralysis.

3.3.1. Steady, Overdamped Response—Steady results of the beam deformation are shown in Figure 11 for the cases of symmetric and asymmetric beam Young's modulus. As E^* increased, deflection of the stiff beam was significantly reduced, but the effect on the other beam was relatively minor.

Figure 12 shows the z-component of the flow velocity, u_3, in the region of the constriction for E^* = 1 and E^* = 2. The jet at the exit was symmetric with E^* = 1, but the asymmetry in beam deflection with E^* = 2 was sufficient to cause the jet to attach to the bottom wall. This tendency of the jet to attach to one wall in this manner is referred to as the "Coanda effect." Because of its influence on the intraglottal pressure distribution, it is of interest to know whether or not the Coanda effect is manifested under physiological conditions. While asymmetry in the jet plume direction occurred in the numerical simulations shown here, further simulations and experiments are necessary to determine the range of conditions under which the Coanda effect becomes significant.

3.3.2. Time-Varying Response—Figure 13 shows the displacement of a point on each beam vs. time for E^* = 1, 2, and 10. The points correspond to the location of the beams closest to the x = 0 centerline in the steady-state solution; the coordinates of the points at t = 0 on the top and bottom beams, (x_L, z_L) and (x_R, z_R), respectively, are listed in Table 2.

Self-sustained oscillations were achieved for $E^* = 2$, although the amplitude was reduced. The bottom beam oscillation amplitude was approximately one-third of the $E^* = 1$ amplitude, and the top beam oscillations were approximately half as great as the bottom beam oscillations. The frequency of the top beam (which was twice as stiff as the bottom beam) fluctuated initially, but eventually matched that of the lower beam. The frequency of oscillation was nearly the same as that for $E^* = 1$. For $E^* = 10$, the oscillations were no longer self-sustained. This was attributed to the larger orifice width caused by the stiffer top beam, resulting in the onset pressure of the system increasing beyond 30 Pa.

4. Conclusions

A numerical model of the vocal fold cover, including the epithelium and the lamina propria, was introduced. This model was similar to cases that have been studied previously in which a compliant beam is placed in a collapsible channel wall and a constant pressure is applied to the beam exterior. The present case differed by the introduction of a fluid-filled cavity on the beam exterior. The compliant section of the wall was highly constricted to simulate the laryngeal constriction caused by the vocal folds.

Steady beam deformation positions were achieved by defining a high cavity fluid viscosity. In these simulations, the steady position was accompanied by a uniform cavity pressure. For lower cavity fluid viscosity and sufficiently high upstream pressure, beam vibrations resulted. For these cases, the cavity pressure experienced significant fluctuations, resulting in an unsteady and non-uniform pressure loading condition.

Both steady and unsteady beam deformations included the presence of an inflection point on the beam, with the upstream region of the beam expanding outwards and the downstream region of the beam constricting inwards. This differed from previous constant-pressure collapsible channel studies, in which low pressures often resulted in constriction of the entire beam surface. In the present cases, incompressibility of the cavity region required that constriction of any portion of the beam be accompanied by expansion of another region of the beam.

The numerical model oscillated at a frequency slightly lower and at an onset pressure significantly lower than typical human speech. The lower onset pressure was a consequence of energy losses in the numerical model being confined to viscous losses within the fluid domain. It was shown that in cases of asymmetric beam stiffness, the orifice jet was asymmetric and the oscillation amplitude decreased. For severe cases of beam asymmetry, oscillations ceased altogether.

Several areas of further work would be beneficial to further characterize this model. These include explorations of the influence of structural damping, of fluid cavity size, of reduction in beam stiffness, and of the flow and structural conditions for which the Coanda effect becomes significant.

Acknowledgments

This work was supported by NIH Grants NIDCD R01 DC03577 and R01 DC05788. The first author also acknowledges the support of a National Science Foundation Graduate Research Fellowship.

References

1. Luo XY, Pedley TJ. A numerical simulation of steady flow in a 2-D collapsible channel. J Fluids Structures. 1995; 9(2):149–174.

2. Luo XY, Pedley TJ. A numerical simulation of unsteady flow in a 2-D collapsible channel. J Fluid Mech. 1996; 314:191–225.
3. Pedley TJ, Luo XY. Modelling flow and oscillations in collapsible tubes. Theoret Comp Fluid Dynamics. 1998; 10:277–294.
4. Luo XY, Pedley TJ. The effects of the wall inertia on the 2-D collapsible channel flow. J Fluid Mech. 1998; 363:253–280.
5. Luo XY, Pedley TJ. Flow limitation and multiple solutions in 2-D collapsible channel flow. J Fluid Mech. 2000; 420:301–324.
6. Cai ZX, Luo XY. A fluid-beam model for flow in collapsible channels. J Fluid Structures. 2003; 17:123–144.
7. Shim EB, Kamm RD. Numerical simulation of steady flow in a compliant tube or channel with tapered wall thickness. J Fluids Structures. 2002; 16(8):1009–1027.
8. Kaazempur-Mofrad MR, Bathe M, Karcher H, Younis HF, Seong HC, Shim EB, Chan RC, Hinton DP, Isasi AG, Upadhyaya A, Powers MJ, Griffith LG, Kamm RD. Role of simulation in understanding biological systems. Computers & Structures. 2003; 81:715–726.
9. Marzo A, Luo XY, Bertram CD. Three-dimensional flow through a thick-walled collapsible tube. J Fluids Structures. 2005; 20:817–835.
10. Hirano, M.; Kakita, Y. Cover-body theory of vocal fold vibration. In: Daniloff, R., editor. Speech Science. College-Hill Press; San Diego, CA: 1985. p. 1-46.
11. Thomson SL, Mongeau L, Frankel SH. Aerodynamic transfer of energy to the vocal folds. J Acoust Soc Am. 2005; 118:1689–1700. [PubMed: 16240827]
12. Titze IR, Schmidt SS, Titze MR. Phonation threshold pressure in a physical model of the vocal fold mucosa. J Acoust Soc Am. 1995; 97:3080–3084. [PubMed: 7759648]
13. Chan RW, Titze IR, Titze MR. Further studies of phonation threshold pressure in a physical model of the vocal fold mucosa. J Acoust Soc Am. 1997; 101:3722–3727. [PubMed: 9193059]
14. Chan RW, Titze IR. Dependence of phonation threshold pressure on vocal tract acoustics and vocal fold tissue mechanics. J Acoust Soc Am. 2006; 119(4):2351–2362. [PubMed: 16642848]
15. Ishizaka K, Flanagan JL. Synthesis of voiced sounds from a two-mass model of the vocal cords. Bell Syst Tech J. 1972; 51:1233–1268.
16. Alipour F, Berry DA, Titze IR. A finite-element model of vocal-fold vibration. J Acoust Soc Am. 2000; 108:3003–3012. [PubMed: 11144592]
17. De Oliveira Rosa M, Pereira JC, Grellet M, Alwan A. A contribution to simulating a three-dimensional larynx model using the finite element method. J Acoust Soc Am. 2003; 114:2893–2905. [PubMed: 14650023]
18. Decker G, Thomson SL. Computational simulations of vocal fold vibration: Bernoulli vs. Navier-Stokes. J Voice. (in press).
19. Thomson, SL. PhD Thesis. Purdue University; West Lafayette, IN: 2004. Fluid-Structure Interactions Within the Human Larynx.
20. Kakita, Y.; Hirano, M.; Ohmaru, K. Physical properties of the vocal fold tissue: Measurements on excised larynges. In: Stevens, KN.; Hirano, M., editors. Vocal Fold Physiology. University of Tokyo Press; Tokyo: 1981. p. 377-396.
21. Chan, RW. personal communication. 2004.
22. Bathe, KJ. Finite Element Procedures. Prentice Hall; New Jersey: 1996.
23. Rugonyi S, Bathe KJ. On the Finite Element Analysis of Fluid Flows Fully Coupled with Structural Interactions. Computer Modeling in Engineering & Sciences. 2001; 2:195–212.
24. Rugonyi S, Bathe KJ. An Evaluation of the Lyapunov Characteristic Exponent of Chaotic Continuous Systems. Int Journal for Numerical Methods in Engineering. 2003; 56:145–163.
25. Bathe KJ, Zhang H. Finite Element Developments for General Fluid Flows with Structural Interactions. Int Journal for Numerical Methods in Engineering. 2004; 60:213–232.
26. Titze IR. The physics of small-amplitude oscillation of the vocal folds. J Acoust Soc Am. 1988; 83:1536–1552. [PubMed: 3372869]
27. Lucero JC. Relation between the phonation threshold pressure and the prephonatory glottal width in a rectangular glottis. J Acoust Soc Am. 1996; 100(4):2551–2554. [PubMed: 8865659]

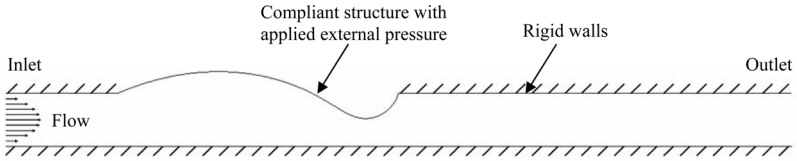

Figure 1.
Illustration of the classical case of a compliant structure in a channel wall.

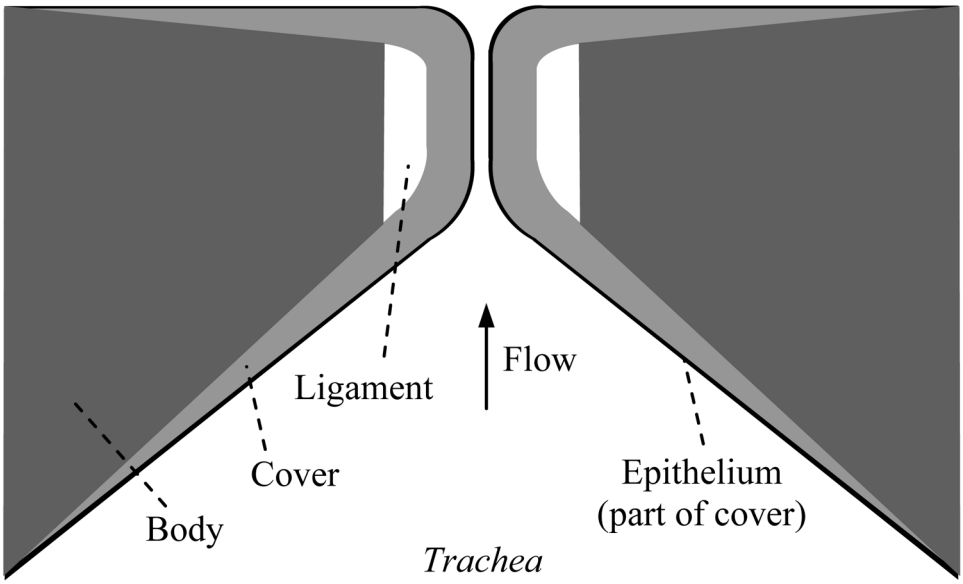

Figure 2.
Sketch of a cross-section of the vocal folds, showing the cover, ligament, and body layers.

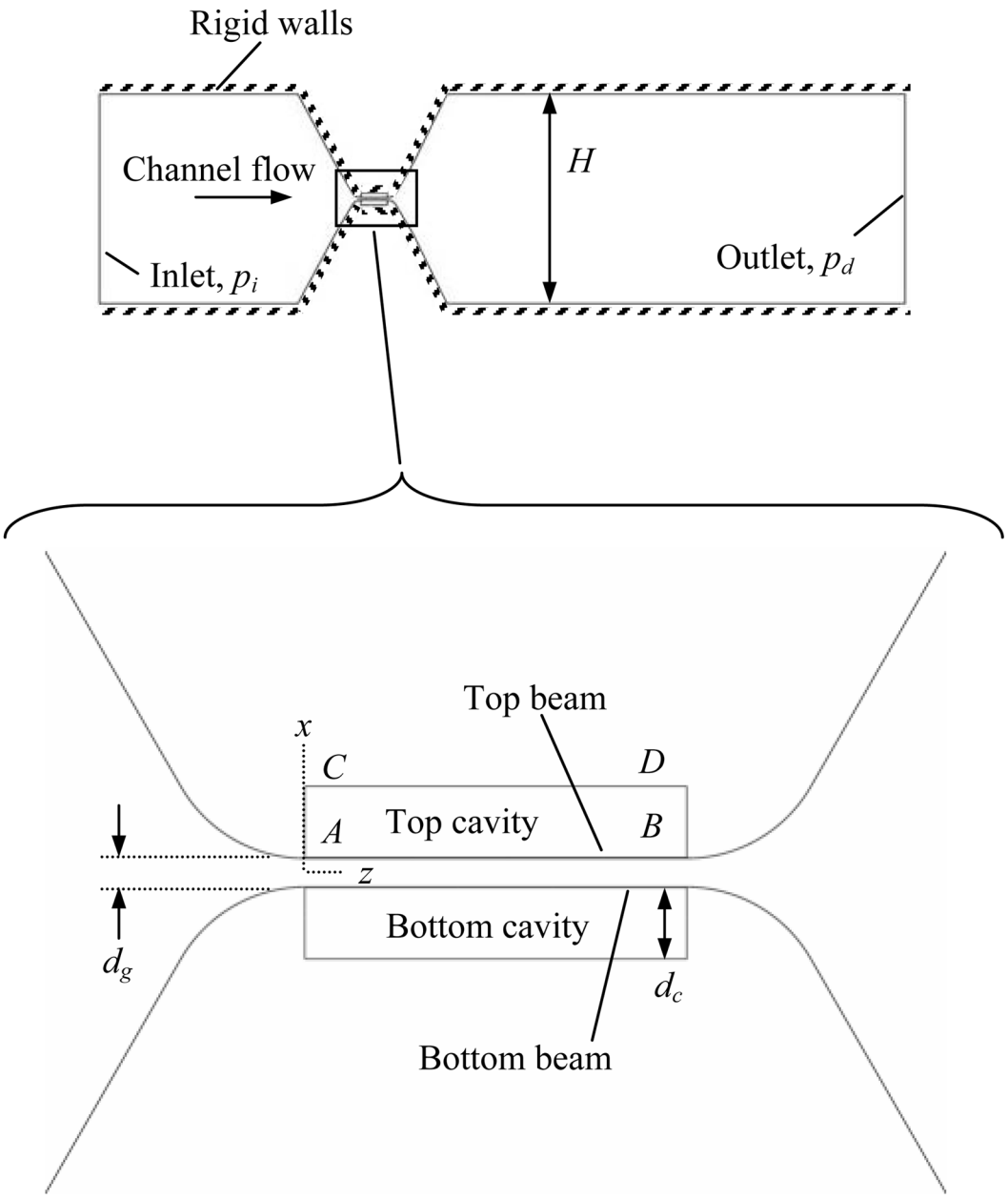

Figure 3.
Channel, cavity, and beam computational domains.

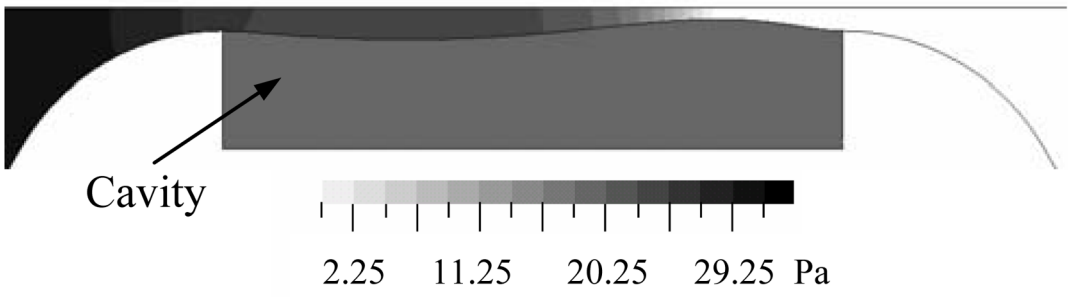

Figure 4.
Fluid-loaded beam steady pressure contours.

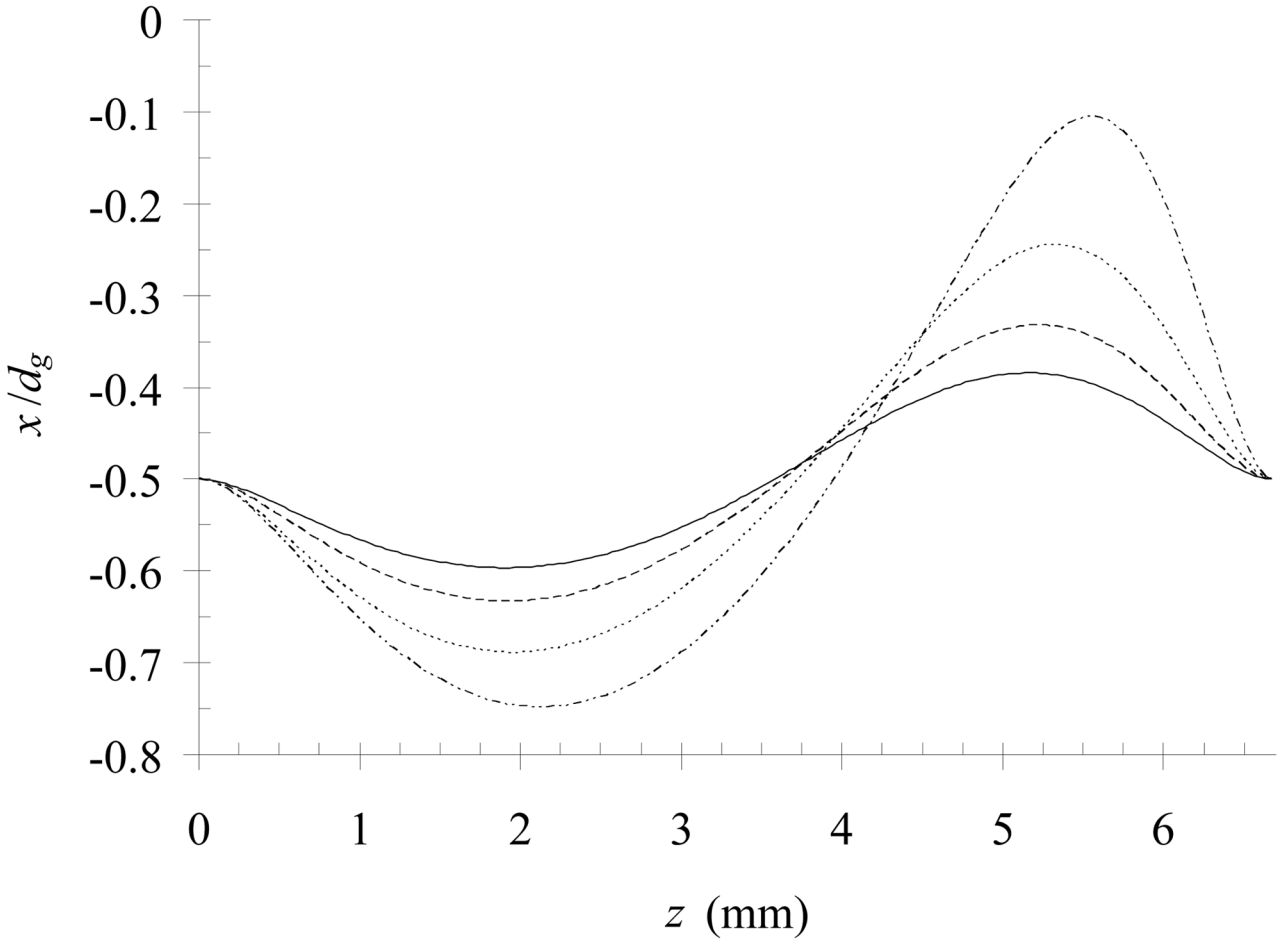

Figure 5.
Steady state beam height for different values of initial gap width with p_s = 30 Pa. ——: d_g = 1 mm; – – –: d_g = 0.75 mm; ···: d_g = 0.5 mm; – ·· –: d_g = 0.25 mm. The centerplane is along x/d_g = 0.

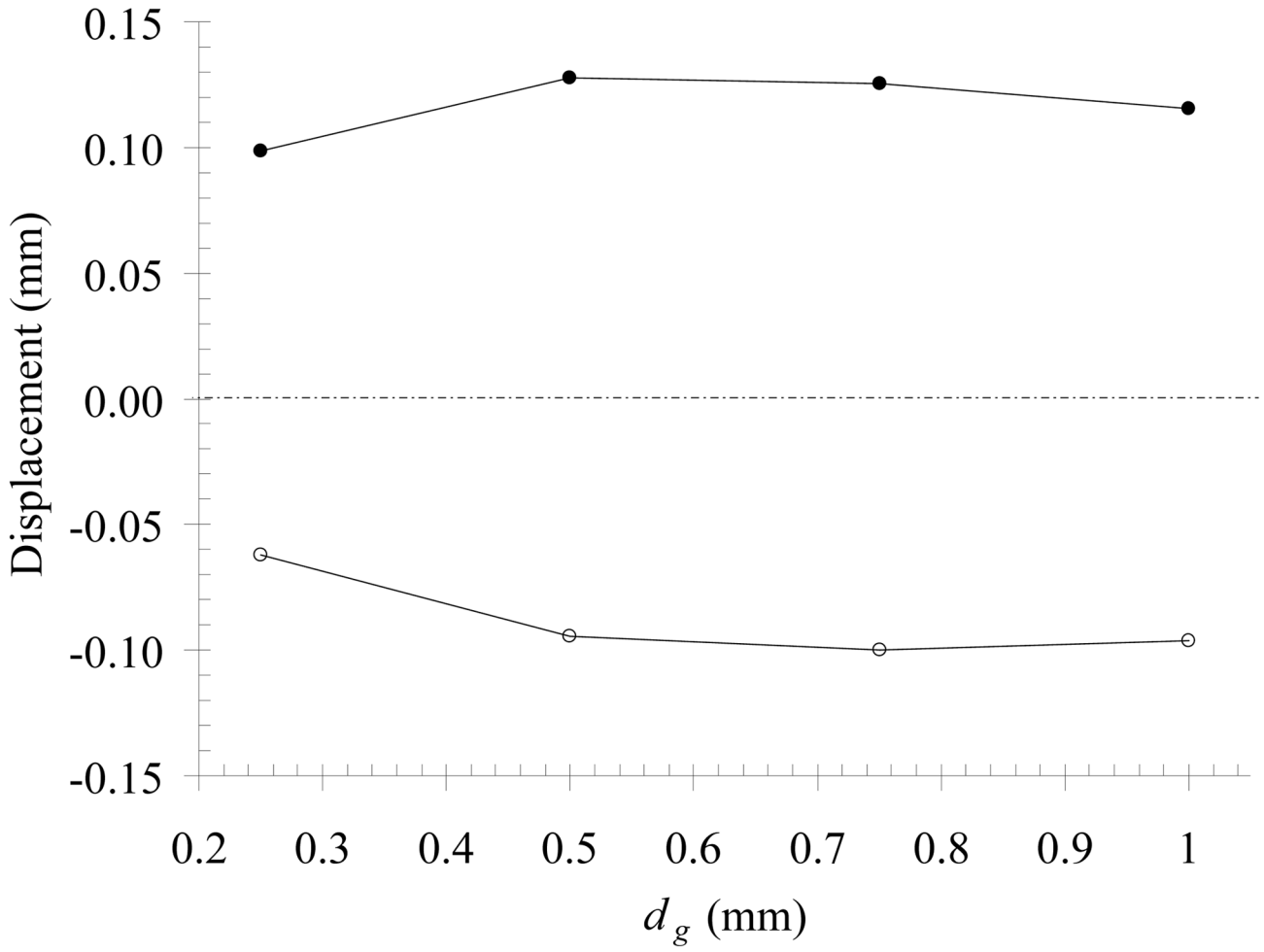

Figure 6.
Maximum and minimum displacement values for different values of d_g with p_s = 30 Pa. –●–: Maximum displacement; –○–: Minimum displacement.

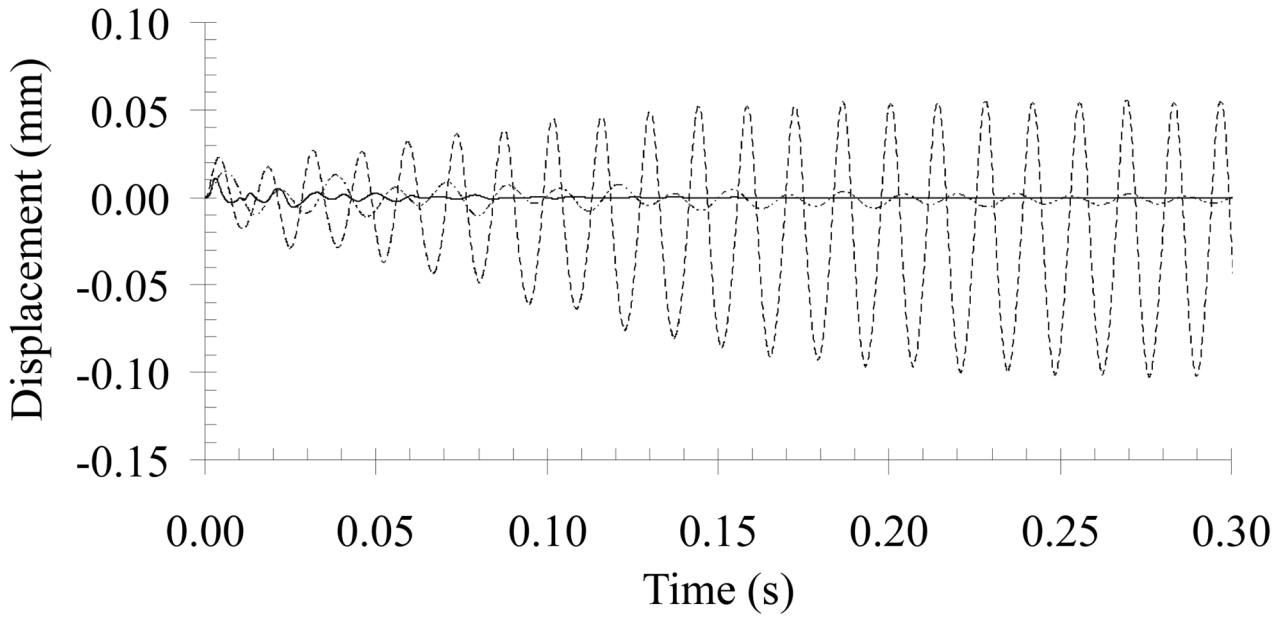

Figure 7.
Unsteady beam position for different values of d_g with p_s = 30 Pa. ——: d_g = 0.25 mm; – – –: d_g = 0.5 mm; – ·· –: d_g = 1 mm.

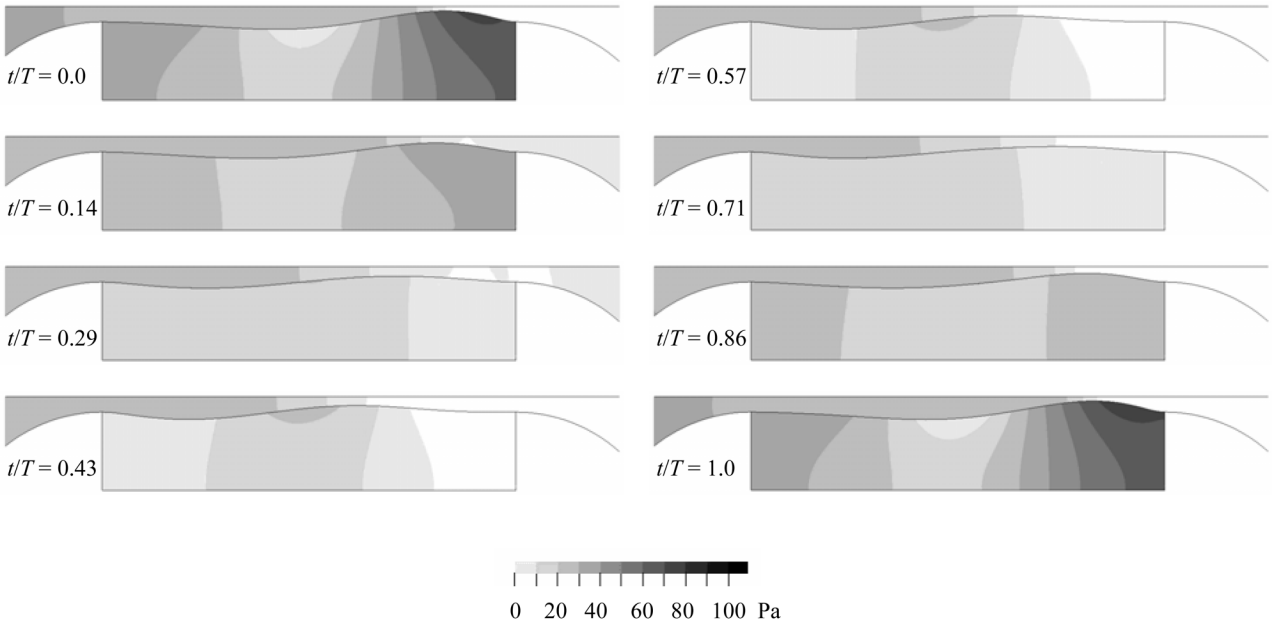

Figure 8.
Pressure contours at different times during one oscillation cycle, obtained with p_s = 30 Pa and d_g = 0.5 mm.

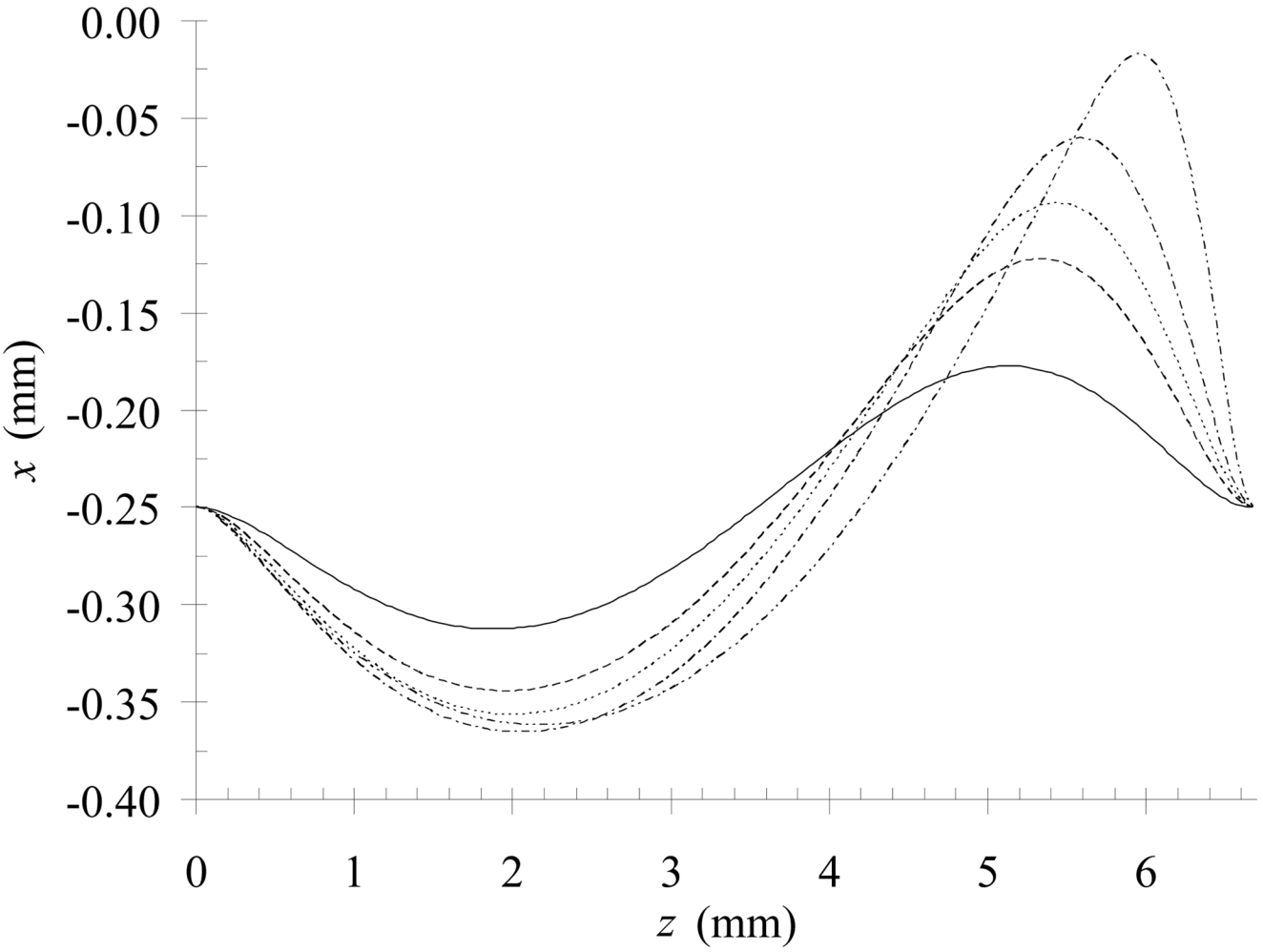

Figure 9.
Beam height for different values of p_s with d_g = 0.5 mm. The location x = 0 corresponds to the center plane. ——: p_s = 10 Pa; – – –: p_s = 30 Pa; ···: p_s = 50 Pa; – · –: p_s = 100 Pa; – ·· –: p_s = 500 Pa.

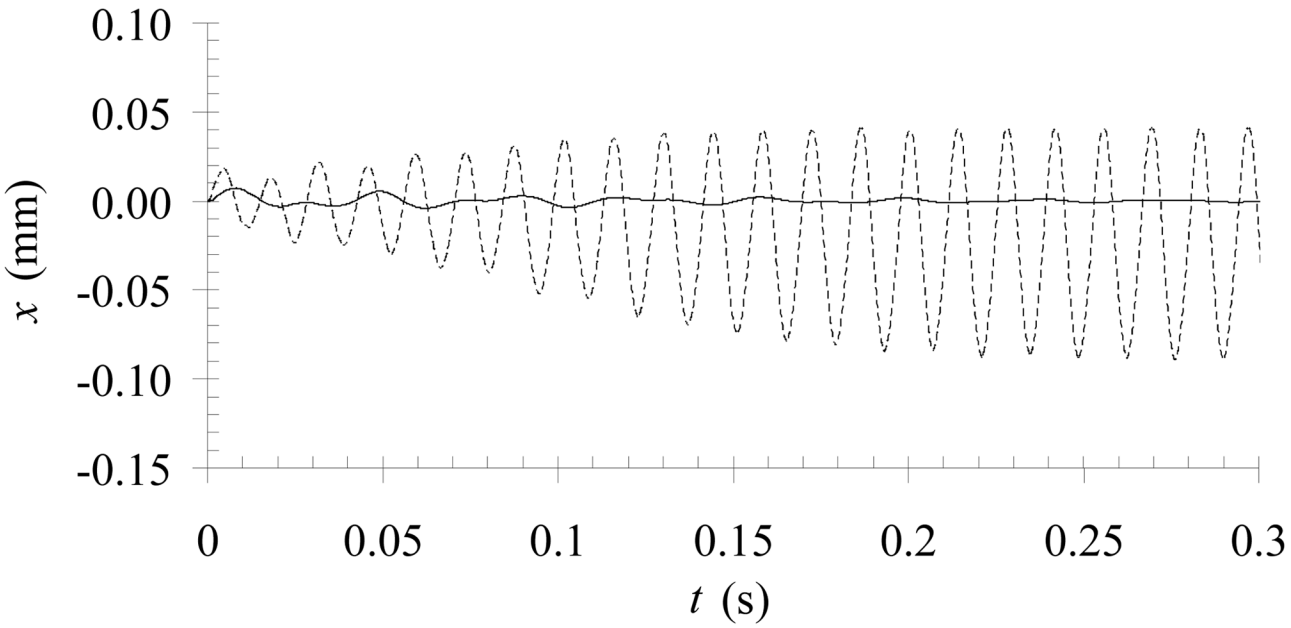

Figure 10.
Unsteady wall position for two different values of p_s with d_g = 0.5 mm. ——: p_s = 10 Pa; – – –: p_s = 30 Pa.

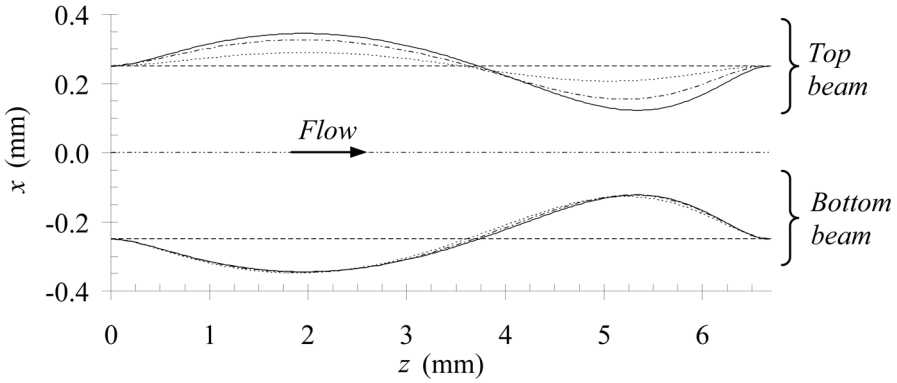

Figure 11.
Steady position of the deformed beams for d_g = 0.5 mm, p_s = 30 Pa, and asymmetric beam Young's moduli. ——: E^* = 1; – · –: E^* = 2; ···: E^* = 10; – – –: Undeformed beam position; – ·· –: Centerplane.

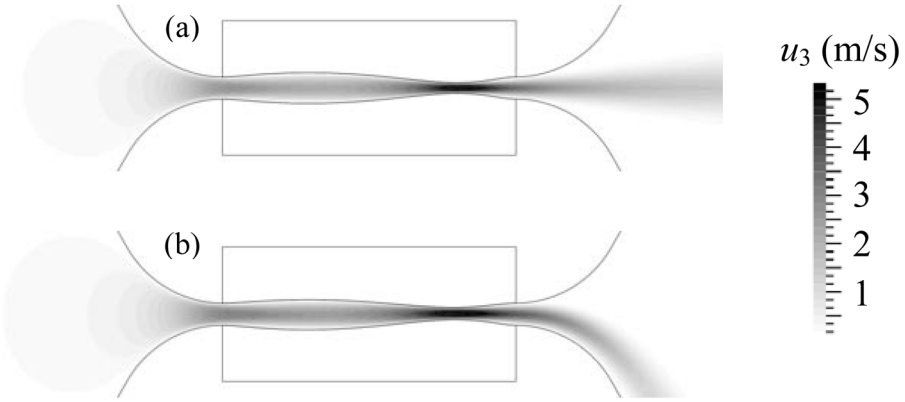

Figure 12.
Contours of the *z*-component of velocity, u_3. (a) $E^* = 1$ (symmetric); (b) $E^* = 2$.

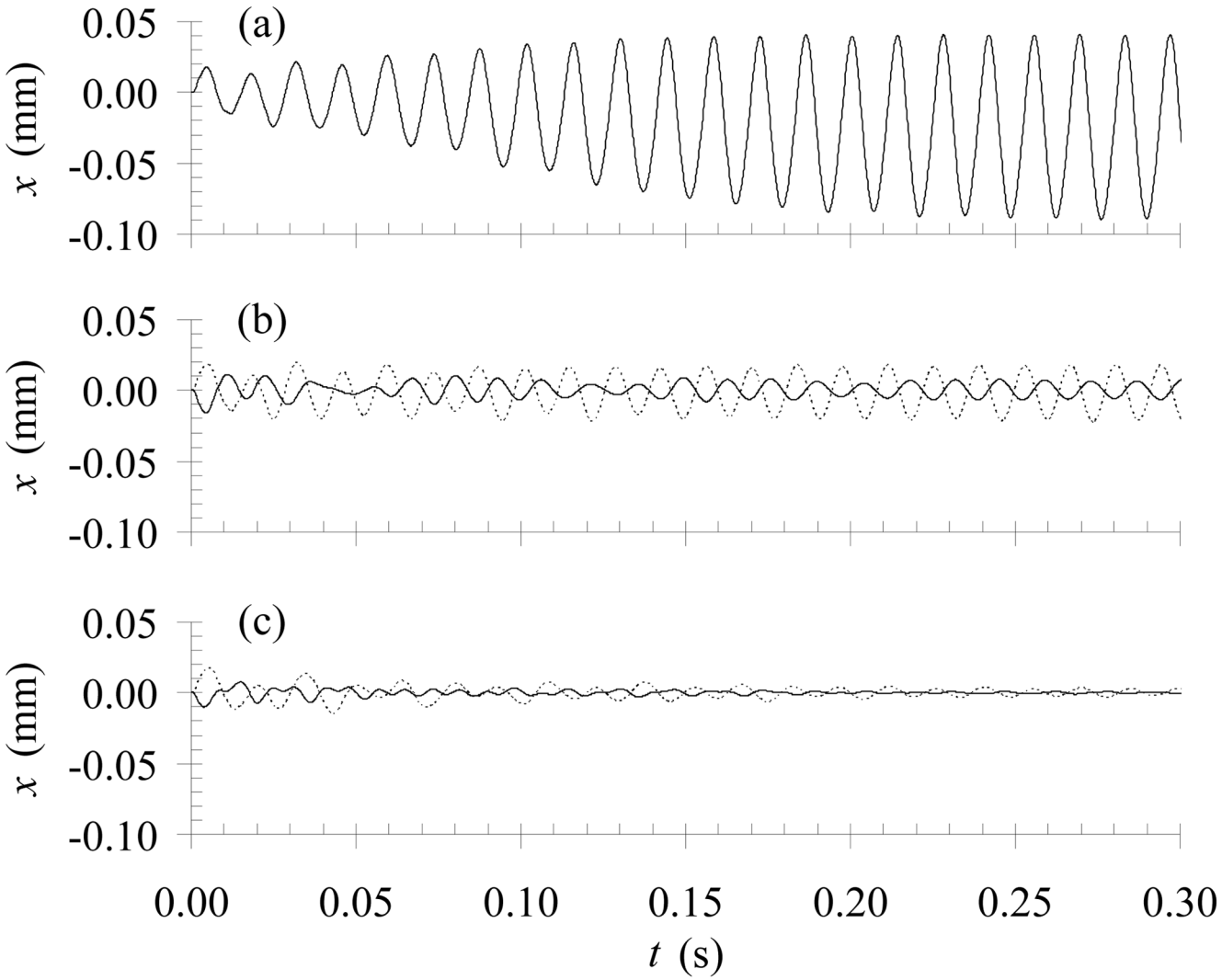

Figure 13.
Displacement displacement vs. time for the points on the beam listed in Table 2. (a) E^*= 1 (symmetric); (b) E^* = 2; (c) E^* = 10. ——: x_T; ···: x_B.

Table 1

Parameter values for the numerical studies.

Parameter	Description	Value
ρ_p	Channel fluid density	1.2 kg/m^3
ρ_c	Cavity fluid density	1000 kg/m^3
ρ_s	Beam density	1000 kg/m^3
μ_p	Channel fluid viscosity	1.8×10^{-5} kg/(ms)
μ_c	Cavity fluid viscosity	0.1 – 0.001 kg/(ms)
ν	Beam Poisson's ratio	0.45
d_b	Beam thickness	0.05 mm
d_g	Glottal gap	0.25 – 1 mm
d_c	Cavity depth (x-direction)	1.25 mm
E_T	Top beam modulus	5×10^5 – 5×10^6 Pa
E_B	Bottom beam modulus	5×10^5 Pa
H	Inlet, outlet duct height	5.4 cm
L_b	Beam & cavity length	6.7 mm
L_d	Downstream duct length	30 cm
L_u	Upstream duct length	6.6 cm
p_d	Outlet pressure	0 Pa
p_i	Inlet pressure	10 – 500 Pa

Table 2

Coordinates at time $t = 0$ of the points plotted in Figs. 10 and 13.

E^*	(x_L, z_L)	(x_R, z_R)
1	(−0.123, 5.34)	(0.123, 5.34)
2	(−0.154, 5.20)	(0.123, 5.27)
10	(−0.206, 5.05)	(0.128, 5.22)